Laminar specificity of functional MRI onset times during somatosensory stimulation in rat

Afonso C. Silva* and Alan P. Koretsky

Laboratory of Functional and Molecular Imaging, National Institute of Neurological Disorders and Stroke, Bethesda, MD 20892

Communicated by Leslie G. Ungerleider, National Institutes of Health, Bethesda, MD, September 17, 2002 (received for review March 7, 2002)

The blood oxygenation level-dependent (BOLD) response to somatosensory stimulation was measured in α-chloralose-anesthetized rats. BOLD fMRI was obtained at 40-ms temporal resolution and spatial resolution of 200 × 200 × 2,000 μm^3 by using a gated activation paradigm in an 11.7 T MRI. Results show a consistent heterogeneity of fMRI onset times and amplitudes. The earliest onset time (0.59 ± 0.17 s, $n = 9$) corresponded anatomically to layer IV, with superficial and deeper layers starting significantly later (1.27 ± 0.43 s in layers I–III, and 1.11 ± 0.45 s in layer VI). The amplitude of BOLD signal changes also varied with the cortical depth from the pial surface. Changes in the supragranular layers (8.3%) were 44% bigger than changes in the intermediate layers (5.5%), located only ≈700 μm below, and 144% larger than the bottom layer (3.5%), located ≈1.4 mm below the pial surface. The data presented demonstrate that BOLD signal changes have distinct amplitude and temporal characteristics, which vary spatially across cortical layers.

Functional MRI techniques based on either changes in blood oxygenation, regional cerebral blood flow (rCBF), or regional cerebral blood volume (rCBV) are having a large impact in defining regions of the brain that are activated by a large variety of tasks (1). With the advent of event-related functional MRI (fMRI) there has been increasing interest in defining the time course of fMRI responses in different areas of the brain to attempt to put a temporal order on areas that are activated (2–4). Stimuli as short as 50 ms have been shown to give fMRI responses and careful analysis of onset times of fMRI responses have detected differences between regions on the order of 100 ms (5). A recent report uses a clever inhibitory circuit to time neuronal events on the order of milliseconds by using fMRI (6). Along with the push to more fully analyze temporal fMRI responses there has been a push to higher spatial resolution to map subregions within activated areas. For example, there are reports that have detected spatial heterogeneity of fMRI that are attributed to ocular dominance or orientation columns in both human (7–10) and cat visual cortex (11, 12). Mapping of single digits within sensorimotor regions (13) and different auditory tones in auditory cortex have been reported in the human (14–16). In animal models, mapping of single whisker barrels has been accomplished in the rat (17). All of this work continues to demonstrate a high spatial and temporal specificity for fMRI techniques.

The rat somatosensory cortex has been an excellent model system to investigate issues related to fMRI. A number of groups have reported robust fMRI responses to forepaw stimulation with general agreement about the area activated and extent of activation (18–21). Work in the rodent model has been performed at relatively high temporal and spatial resolution to address questions of the anatomical origin of fMRI signal, such as large vessel vs. small vessel contribution to blood oxygen level-dependent (BOLD) fMRI (22). In addition, there have been careful comparisons of onset of BOLD, perfusion, and blood volume-based fMRI (23, 24).

The neuronal innervation in the case of forepaw stimulation is well known. Most afferents from the thalamus innervate the somatosensory cortex at layer IV with excitation going up to layers III–I and down to layers V–VI (25). Electrical recording from these layers indicate that there is about a 3–4 ms delay of activation from onset in layer IV to activating other layers (26). We have studied onset times to forepaw stimulation in the rat somatosensory cortex. BOLD fMRI were obtained at 40 ms temporal resolution and spatial resolution of 200 × 200 × 2,000 μm^3 by using a gated activation paradigm in an 11.7 T MRI. Results clearly show a consistent heterogeneity of fMRI onset times, with the earliest regions to activate corresponding anatomically to layer IV. These results open up the possibility of using fMRI to monitor laminar communication within areas of the brain.

Methods

Animal Preparation. This study was conducted on nine male adult Sprague–Dawley rats, weighing 245 ± 64 g. Surgical procedures were performed under halothane anesthesia (5% induction, 1.5% maintenance). The rats were orally intubated and mechanically ventilated throughout the experiments. Plastic catheters were inserted in the right femoral artery and vein. After surgery, the rats were placed in a home-built head holder and a 1.6-cm-diameter surface coil was positioned on top of the head over bregma and secured to the head holder. Animals were positioned and strapped to a semicylindrical cradle. Rectal temperature was maintained close to 37°C by means of a heated water blanket. Halothane was discontinued and anesthesia was switched to α-chloralose (80 mg/kg initially, followed by a constant infusion of 26.7 mg/kg/hr) throughout the remainder of the experiment. Pancuronium bromide was administered intravenously at doses of 4 mg/kg every 90 min to aid with immobilization. Rectal temperature, end-tidal CO_2, tidal pressure of ventilation, arterial blood pressure, and heart rate were recorded throughout the experiments. Blood gases were adjusted and monitored throughout the experiments. Arterial blood pH was 7.26 ± 0.06, PaCO2 was 35.7 ± 6.4 mmHg, and PaO2 was 105 ± 16 mmHg.

Forepaw Stimulation. Two needle electrodes were inserted under the skin of the left forepaw (in the space between digits 2 and 3, and 4 and 5). Stimulation parameters were: current intensity, 2 mA; frequency, 3 Hz; and pulse duration, 0.3 ms (21).

fMRI Methods. All images were acquired using an 11.7 T/31 cm horizontal magnet (Magnex, Abingdon, U.K.), interfaced to an AVANCE console (Bruker, Billerica, MA). The imaging slice over the somatosensory cortex, about 0–1 mm rostral to bregma, was chosen based on preacquired tri-pilot spin-echo scout images. Single-average, conventional gradient-echo images were obtained from a 2-mm-thick coronal plane and a 1.28 × 1.28 cm^2 field-of-view, corresponding to nominal in-plane resolutions of either 200 × 200 μm^2, using a 64 × 64 matrix, or 50 × 50 μm^2, using a 256 × 256 matrix. In all cases, TR/TE = 40/10 ms were used, and the flip angle was adjusted to maximize signal. Three different stimulation paradigms were used:

Abbreviations: BOLD, blood oxygenation level-dependent; CCC, cross-correlation coefficient; fMRI, functional MRI; ROI, region of interest.

*To whom correspondence should be addressed at: Laboratory of Functional and Molecular Imaging, National Institute of Neurological Disorders and Stroke, 10 Center Drive, Building 10/B1D118, Bethesda, MD 20892-1065. E-mail: silvaa@ninds.nih.gov.

 www.pnas.org/cgi/doi/10.1073/pnas.222561899

1. The region of activation was verified using a baseline–stimulus–baseline paradigm at the lower in-plane resolution of 200 × 200 μm^2 with the initial baseline period of 60 s (24 images), followed by a 30-s stimulation period (12 images), and finalizing with a 60-s period (24 images) to allow the signal to return to baseline.
2. An experiment was performed at 50 × 50 μm^2 in-plane resolution by using a paradigm of 4 min baseline (24 images), followed by a 2-min-long stimulus (12 images), and ending with a resting period of 4 min (24 images).
3. The scan for the onset time maps was acquired using a 64 × 64 matrix (200 × 200 μm^2 in-plane resolution). A total of 750 images (total scan time of 32 min) were acquired. To obtain an effective temporal resolution of 40 ms per frame, the order of the phase-encoding and the repetition loops was exchanged so that the same line in k-space would be acquired for all 750 images (total of 30 s per k-space line) before incrementing the phase-encoding gradient to the next line. The stimulation period was locked-in to the scan of each line in k-space, so that the initial 100 images (4 s) were acquired during stimulation and the remaining 650 images (26 s) were acquired in the resting state. Therefore, 64 stimulation epochs, each lasting 30 s, were necessary to complete the scan of the 64 k-space lines. Two-dimensional Fourier reconstruction was performed on each image after rearranging the data so that a single time course consisting of the bulk average response to the 64 stimulation epochs was obtained. This gave an effective temporal resolution of 40 ms to follow the BOLD time courses.

Following the 32-min acquisition of the onset time maps, the initial 60 s–30 s–60 s off–on–off paradigm was repeated at 200 × 200 μm^2.

MRI Data Analysis. The functional images acquired under all three paradigms were processed using a boxcar cross-correlation method (27). Activation maps were generated from pixels presenting a minimum cross-correlation coefficient (CCC) value of 0.3. Further analysis of the high temporal resolution data (paradigm 3) was constrained only to pixels in these cross-correlation maps. The time course of each of the active pixels was low-pass filtered with a Hanning window to remove periodical susceptibility artifacts induced by mechanical ventilation of the animals. A t value was obtained at each time point for each active pixel by using as baseline the last 4 s of data acquired immediately before the 4 s stimulus. For the purposes of defining onset times, the mean and the standard deviation of each pixel was calculated during the baseline period. Pixels were considered active when their t values were more than 1 SD above the baseline mean. Latencies to 10%, 50%, and 100% (time to peak) of the peak positive response were also recorded.

To compare relative BOLD changes across different layers, region of interest (ROI) analysis was performed on the onset time maps. The ROIs were picked based on the anatomical description of the cortical layers of the rat brain (28). To avoid uncertainties in the definition of ROIs containing single cortical layers, the somatosensory cortex was divided into three roughly equal regions, and six pixels from each layer following a column along the center of the activated cortex were assigned for further analysis. The first ROI included only the active pixels located along the top layers (I–III) of the cortex, situated 0–400 μm below the pial surface. The second ROI was located medially in the cortex, along layers IV–V (600–1,000 μm below the pial surface). The third ROI contained the pixels located along the bottom layer (VI) of the cortex (1,400–1,800 μm below the pial surface). For each animal, layer-specific onset times were obtained by averaging all pixels from each ROI.

Data in text and figures are presented as mean ± SD. Student's t tests were performed to compare differences. Differences were considered statistically significant for P values <0.05.

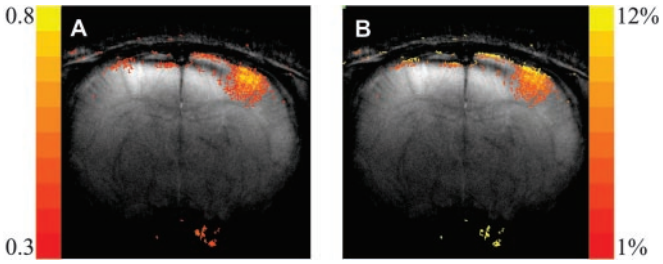

Fig. 1. Typical gradient-echo coronal MR images of a rat brain obtained at 11.7 T. Spatial resolution is 50 × 50 × 2,000 μm^2. Overlaid on top of the images are functional maps generated during electrical stimulation of the left forepaw. (*A*) Cross-correlation map shows the temporal resemblance of each pixel time course to the functional paradigm. The color bar indicates the scale of CCCs. Pixels that best resemble the functional paradigm are located in the middle layers (IV–V) of the somatosensory cortex. (*B*) Percent change map shows the intensity of BOLD relative signal changes. The color bar indicates the range of signal changes. The highest signal changes are located along the pial surface, corresponding to the extravascular component associated with large vessels.

Results

Characteristics of the BOLD Response at High Spatial Resolution. Fig. 1 shows typical gradient-echo coronal MR images of a rat brain (rat 9), obtained at 11.7 T. The image was acquired at 50 × 50 × 2,000 μm^3 spatial resolution. Functional maps generated during electrical stimulation of the left forepaw are shown overlaid on top of the image. In Fig. 1*A*, the cross-correlation map shows the temporal resemblance of each pixel time course to the functional paradigm. Pixels that best resemble the functional paradigm are located in the middle layers (IV–V) of the somatosensory cortex. In Fig. 1*B*, the percent map shows the intensity of BOLD relative signal changes. The highest signal changes are located along the pial surface, corresponding to the BOLD contribution from large pial veins to extravascular signal increases (22). Intermediate signal changes are located in the middle cortical layers, whereas the lowest changes seem to occur in the bottom layer of the cortex.

Fig. 2 show the corresponding BOLD time courses obtained from the experiment shown in Fig. 1. The stimulation paradigm consisted of 60 images, acquired at 10-s temporal resolution: 24 images acquired as a prestimulus baseline, followed by 12 images acquired during forepaw stimulation, and ending with 24 images acquired as the signal returned to baseline. Each BOLD time course was

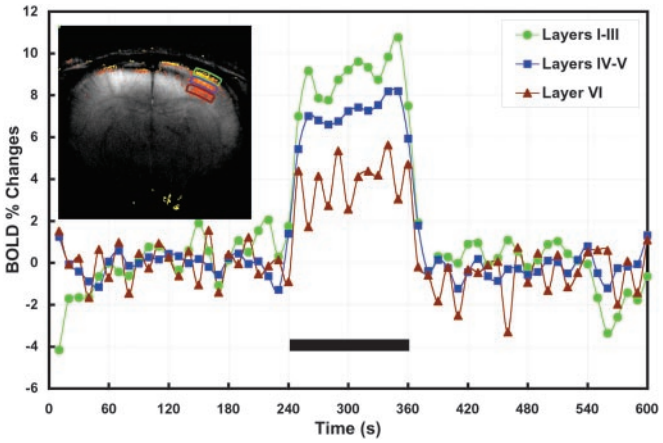

Fig. 2. Laminar heterogeneity of BOLD signal changes. Temporal resolution is 10 s per point. The black bar indicates stimulation period. Three BOLD time courses are shown, obtained from equally sized ROIs chosen according to the anatomical description of the rat cortical layers. The top ROI, in green, contains pixels from layers I–III. The ROI in the middle, shown in blue, contains pixels located in layers IV–V. The bottom ROI, in brown, contains pixels from layer VI.

NEUROSCIENCE

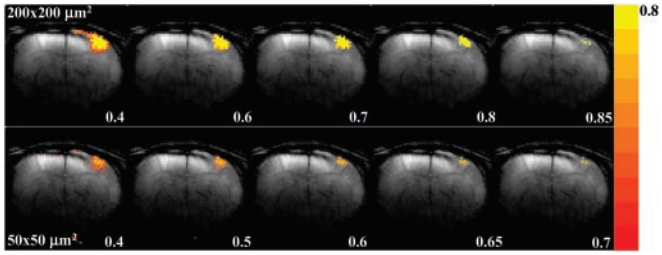

Fig. 3. Cross-correlation BOLD functional maps obtained at 200 × 200 μm^2 (*Upper*) and 50 × 50 μm^2 (*Lower*) in-plane resolution. The color bar indicates the scale of CCC. The upper CCC limit was fixed at 0.8, whereas the lower CCC limit increases from left to right. At either resolution, as the minimum CCC threshold is increased the functional map shrinks to a layer of pixels located 760 ± 89 μm below the pial surface in cortical layer IV.

extracted from equally sized ROIs chosen according to the anatomical description of the rat cortical layers. The top ROI, in green, contains pixels from layers I–III, and originates the strongest BOLD response. The ROI in the middle, shown in blue, contains pixels located in layers IV–V. The bottom ROI, in brown, contains pixels from layer VI, and has the weakest BOLD response.

Fig. 3 shows cross-correlation BOLD functional maps obtained at 200 × 200 μm^2 (*Upper*) and 50 × 50 μm^2 (*Lower*) in-plane resolution. The maps were produced by fixing the upper CCC limit at 0.8 while increasing the lower CCC limit from left to right. At either resolution, as the minimum CCC threshold is increased, the functional map shrinks to a layer of pixels located in cortical layer IV (760 ± 89 μm below the pial surface), indicating that layer has the highest resemblance to the stimulation paradigm, i.e., the fastest onset times of activation and deactivation. For any given CCC threshold, the map obtained at 200 × 200 μm^2 appears larger than the one obtained at 50 × 50 μm^2. This is because of the higher signal-to-noise ratio (SNR) at lower spatial resolution.

Laminar Specificity of BOLD Signal Changes. Table 1 shows the BOLD percent signal changes obtained at a higher (50 × 50 μm^2) and lower (200 × 200 μm^2) in-plane resolution for the three laminar regions considered in this study. The high-resolution scan used a 120-s stimulus period, and produced the same BOLD percent changes as the lower-resolution scans with a 30-s stimulus paradigm. In addition, no changes in BOLD signal changes were observed between the 30-s stimulus paradigms obtained before and after the 32-min-long onset time map scan (data not shown). To further verify the reproducibility of the BOLD response to each of the 64 stimuli, an experiment was performed at 400 × 400 μm^2 in-plane resolution by using echo-planar imaging, during the same stimulation paradigm used to elicit the onset-time maps. The mean BOLD response in this case was 3.2 ± 0.7%, in proof of the excellent reproducibility of our rat model (data not shown).

Table 1. BOLD percent signal changes obtained at two in-plane resolutions during different stimulation periods

Stimulus	Layers I–III*	Layers IV–V†	Layer VI
50 × 50 μm^2 120 s‡	8.4 ± 3.6	5.7 ± 1.9	3.8 ± 1.1
200 × 200 μm^2 30 s	8.2 ± 4.6	5.4 ± 2.2	3.1 ± 1.0
200 × 200 μm^2 4 s§	4.2 ± 1.8	2.9 ± 1.2	1.6 ± 0.4

*BOLD signal changes in layers I–III are significantly larger than the ones in layers IV–V ($P < 0.01$) and in layer VI ($P < 0.003$) at both spatial resolutions and at all stimulus durations.

†BOLD signal changes in layers IV–V are significantly larger than the ones in layer VI ($P < 0.003$) at both spatial resolutions and at all stimulus durations.

‡For all layers, the BOLD signal changes obtained from the 120-s stimulus period at 50 × 50 × 200 μm^3 were not significantly different from the ones obtained from the 30-s stimulus at 200 × 200 × 2000 μm^3 ($P > 0.08$).

§For all layers, the BOLD signal changes obtained from the 4-s stimulus periods were significantly smaller than the ones obtained from either the 120-s stimulus period ($P < 0.001$) or the 30-s stimulus ($P < 0.008$).

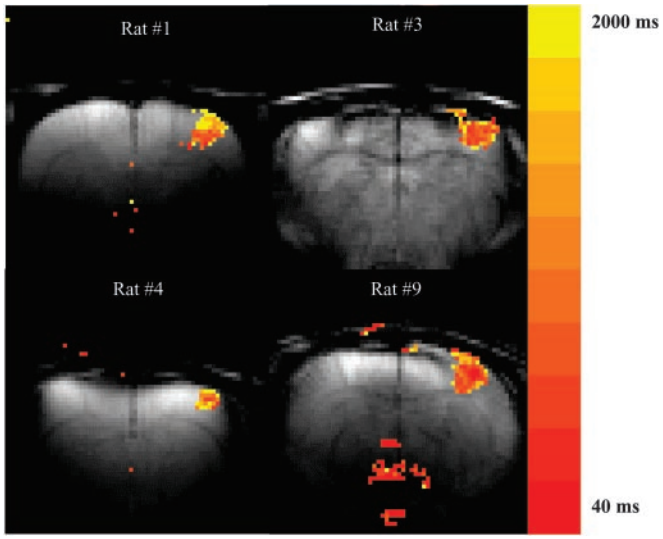

Fig. 4. Typical BOLD onset time maps from four of nine subjects used in this study. The color bar indicates the time scale of activation onset. The fastest onset times come from pixels located in the intermediate layers (IV–V) of the somatosensory cortex, whereas slowest onset times are found in the outer layers (I–III and VI).

It is important to notice that all three paradigms produced BOLD signal changes that have the same region-specific intensity characteristics. The more superficial regions comprised of layers I–III produced the largest BOLD response, followed by the intermediate layers IV–V. The region comprised by layer VI produced the smallest signal changes. BOLD signal changes in layers I–III were 44 ± 31% larger than in layers IV–V, whereas in layer VI they were 37 ± 17% smaller.

BOLD signal changes observed during the 4-s stimulus paradigm were significantly smaller than the responses associated with either the 30-s ($P < 0.008$) or the 120-s ($P < 0.001$) paradigms. This is because a 4-s stimulus is not long enough to elicit a peak response (see below). On the other hand, the intensities of BOLD responses obtained with the longer paradigms (30 s and 120s) were not different from each other ($P > 0.08$).

Laminar Specificity of BOLD Onset Times. Fig. 4 shows typical BOLD onset time maps obtained from four of the nine rats used in this study. Data were obtained as explained in *Methods*. It is evident that the fastest onset times come from pixels located in the intermediate layers (IV–V) of the somatosensory cortex, whereas slowest onset times are found in the outer layers (I–III and VI).

Fig. 5*A* shows high temporal resolution (40 ms per point) BOLD time courses obtained at 200 × 200 μm^2 in-plane resolution from rat 9. Time courses obtained from six-pixel ROIs located in layers I–III, IV–V, and VI (*Inset*) are plotted. It is clear that the time course from layers IV–V (blue) rises monotonically and faster following the start of stimulation than the more delayed and sluggish time courses from layers I–III (green) and layer VI (brown). In addition, an early negative BOLD signal trend was observed in the time courses from layers I–III and VI before the positive response to the stimulus. This negative trend, however, was not consistently observed for every animal, and averaged out below statistical significance.

Fig. 5*B* shows averaged BOLD time courses obtained at 40-ms temporal resolution from all nine animals used in this study. Layers IV–V present the fastest onset time to stimulation, followed by

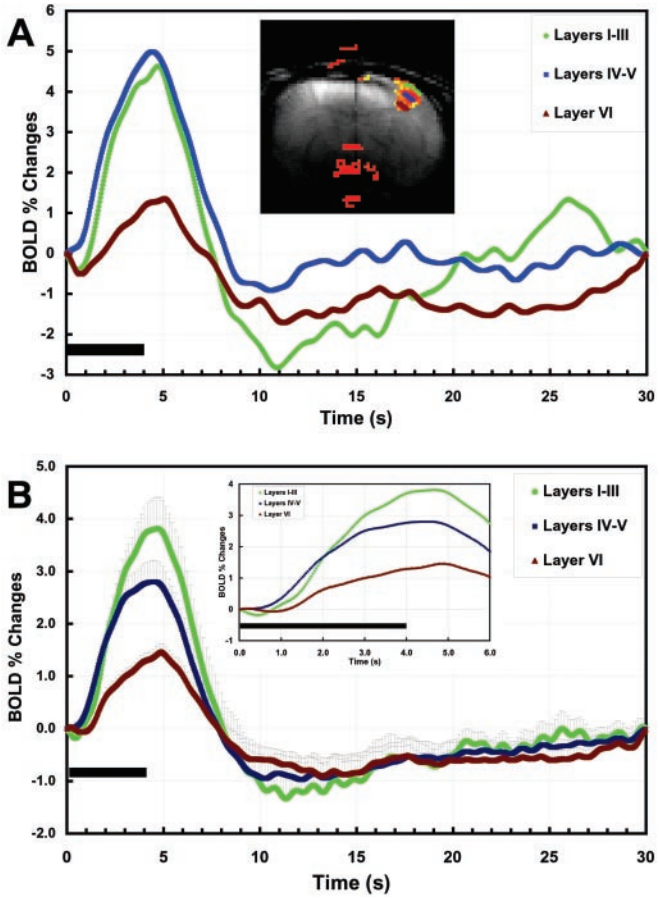

Fig. 5. (*A*) Typical high temporal resolution (40 ms per point) BOLD time courses obtained at 200 × 200 μm^2 in-plane resolution from a single animal (rat 9). The black bar indicates the 4-s stimulus. Sixty-four stimulation epochs were used to acquire these data (see text). Time courses obtained from six-pixel ROIs located in layers I–III, IV–V, and VI (see *Inset*) are plotted in green, blue, and brown, respectively. It can be clearly seen that the BOLD response from layers IV–V rises monotonically and faster than the more delayed time courses from layers I–III and from layer VI, which trend negatively before shooting up in response to the stimulus. (*B*) Averaged BOLD time courses obtained at 40-ms temporal resolution from all nine animals used in this study. Layers IV–V present the fastest onset time to stimulation, followed by layers I–III and VI. Vertical bars = 1 standard error. The *Inset* clearly shows the difference in onset times (error bars omitted for clarity).

layers I–III and VI. The *Inset* clearly shows the difference in onset times. The average onset time for layers IV–V was 0.59 ± 0.17 s, significantly shorter than the onset time for layers I–III, 1.28 ± 0.42 s ($P < 0.001$), as well as the onset time for layer VI, 1.11 ± 0.45 s ($P < 0.003$). The onset time for layers I–III was not significantly different from the one for layer VI ($P > 0.1$). Table 2 shows the average onset times based on the 1 SD criteria, as well as the times to reach 10%, 50%, and 100% of the peak response (time to peak), for each of the three regions considered in this study.

Discussion

Summary of Main Findings. In this study, we measured the hemodynamic response to somatosensory stimulation with high spatial and temporal resolution. BOLD temporal characteristics can be probed by means of cross-correlation analysis and by direct inspection of pixel time courses for amplitude and temporal variation. The amplitude of relative BOLD signal changes was shown to vary with the cortical depth from the pial surface (Table 1; Figs. 1*B*, 2, and 5). The largest signal changes occurs along the supragranular layers, and decreases monotonically with the cortical depth, the weakest

Table 2. Onset, 10%, 50%, and peak response latencies (in s) to somatosensory stimulation

Response latencies	Layers I–III	Layers IV–V*	Layer VI
Onset time	1.27 ± 0.43	0.59 ± 0.17	1.11 ± 0.45
10% of peak	1.25 ± 0.40†	0.66 ± 0.21	1.02 ± 0.39†
50% of peak	2.60 ± 0.41	2.00 ± 0.37	2.46 ± 0.56
Time to peak	4.37 ± 0.48‡	4.13 ± 0.62	4.79 ± 0.51‡

*Onset time, times to 10% and 50% of peak, and time to peak from layers IV–V are significantly faster than the ones from layers I–III ($P < 0.05$) and layer VI ($P < 0.02$).
†Time to 10% of peak from layer VI is significantly faster than layers I–III ($P < 0.04$).
‡Time to peak from layer VI is significantly longer than layers I–III ($P < 0.003$) and layers IV–V ($P < 0.001$).

changes occurring along layer VI. Changes in the supragranular layers (8.3%) were 44% bigger than changes in the intermediate layers (5.5%), located ≈700 μm below, and 144% larger than the bottom layer (3.5%), located ≈1.4 mm below the pial surface.

The temporal resemblance of the BOLD time course to the stimulation paradigm can be probed by cross-correlation analysis (27). The time courses obtained at high temporal resolution and shown in Fig. 5 present the general features of the BOLD response. During onset of stimulation, the BOLD signal rises up to its peak value over a few seconds. The paradigm used here employed a short stimulus duration (4 s), so that the peak response occurs after the stimulus has terminated. The BOLD response then drops down and undershoots below the baseline, before slowly returning to the resting level. Layer-specific heterogeneity is maintained throughout the rising portion of the response, both in amplitude as well as in time. Our data shows that layers IV–V have the strongest temporal resemblance to the stimulation paradigm (Fig. 3). In particular, onset, times to 10% and 50% of peak, and time to peak obtained from layers IV–V are shorter than the respective latencies from layers I–III and VI (Table 2), suggesting that the hemodynamic response originates in this region and propagates from this region toward the supragranular and infragranular layers. This finding is consistent with the hypothesis that changes in CBF start at the site of neural activity and propagate upstream toward the feeding arterioles and arteries (29, 30). The data presented here demonstrates that BOLD signal changes have distinct amplitude and temporal characteristics that vary spatially across the cortical layers.

Comparison to Previous Studies of CBF Heterogeneities. We have previously measured BOLD onset times in the same rat somatosensory stimulation model (24). The onset of the BOLD response in layers IV–V found here, 0.59 ± 0.17 s, was significantly shorter than the one found previously for the deep cortical layers, 1.1 ± 0.3 s. This apparent discrepancy can be easily explained by the much lower spatial resolution of the previous study (470 × 470 μm^2), and by the fact that the "deep" ROI of the previous study included layers IV–VI, making the onset time a weighted average of the values found here for layers IV–V and layer VI.

A recent study using [^{14}C]iodoantipyrine autoradiography of the rat primary somatosensory barrel field has demonstrated that both the resting CBF as well as the functional changes in CBF to whisker stimulation are heterogeneous across cortical layers (31). Most high temporal resolution studies of the hemodynamic response have been measured by laser Doppler flowmetry (LDF) and by optical imaging of intrinsic signals (32–35). These techniques are mostly sensitive to superficial changes in CBF. Most optical studies report onset times of 1–2 s that are consistent with our results for layers I–III (32, 33, 35). Matsuura *et al.* reported an onset time of 0.5 s to electrical stimulation of the hindpaw (34). A recent rat study used a dual-wavelength device equipped with four detector probes to show that changes in blood flow occur first (0.2 ± 0.2 s) in the superficial layer, and travels to the bottom layers, where the onset

time is about 1 s (35). Reasons for discrepancies between this work and data reported here are not clear. However, the LDF work used direct electrical stimulation at the trigeminal nerve, which excites the whole face somatosensory pathway, and therefore is less specific than the forepaw model used here. In addition, the multiprobe, multiwavelength approach used to pull out laminar information has complications, such as defining the precise resolution, size of the probe, or volume of tissue sampled by the LDF device compared with large vessel distribution, wavelength-dependent absorption and back-scatter differences, and amplitude of the laser-Doppler signal with respect to light intensity. Furthermore, work based on laser-Doppler flowmetry does not predict how fMRI would respond because the BOLD signal has blood flow, blood volume, and hemoglobin oxygenation components. Two-photon laser scanning microscopy has excellent depth resolution and is beginning to be applied to monitoring blood flow changes in the somatosensory cortex. Kleinfeld *et al.* (36) used two-photon laser scanning microscopy to image changes in red blood cell velocities in roughly layers I–III in response to whisker and hindpaw stimulation 200–600 μm below the pial surface in rat. They found a weak dependence of red blood cell velocities on cortical depth, with velocities in the deeper vessels tending to be slower than in the more superficial vessels. However, to relate red cell velocities to blood flow changes would require measurement of vessel diameters, as well as an understanding of the relation between red cell velocity and plasma flow.

Spatial and Temporal Heterogeneity of BOLD Signal Changes. Recent technological improvements in MRI hardware have helped push the spatial resolution of fMRI to map subregions within activated areas. Submillimeter spatial resolution has demonstrated regional heterogeneity in functional maps both in animals as well as humans, and is being increasingly used to map specific architectonic subareas within the visual, auditory, somatosensory and motor cortex. At high resolution, whisker barrels in the rat somatosensory cortex (17), ocular dominance columns in the human visual cortex (8–10), and orientation columns in the cat visual cortex (11, 12). All of this work has averaged across cortical layers to gain signal-to-noise. An important issue for work aimed at high-resolution mapping with fMRI is that the spatial specificity of BOLD-based fMRI depends on the magnetic-field strength and the specific type of imaging sequence (37). For example, gradient-echo sequences like the one used in this study are sensitive to extravascular contributions from large draining veins, even at high-fields (22). Therefore, regions showing the highest BOLD signal changes may be spatially removed from the regions of increased neuronal and metabolic activity. Despite these issues, it is clear that BOLD-based fMRI is successful at mapping subregions. The work presented here suggests that cortical layers may also be distinguished with BOLD fMRI techniques.

There has been much interest in relating BOLD and CBF changes during task activation to estimate oxygen consumption. The spatial heterogeneity of BOLD signal changes detected across the laminar organization of the brain raises important concerns regarding the quantification of oxygen consumption changes from BOLD signal changes, because the regions of highest BOLD signal changes may not be those of highest metabolic activity. The large heterogeneity detected in the present work, 144% differences between pial and deep layers, implies that partial volume effects in oxygen consumption measurements need to be considered.

The laminar heterogeneity of BOLD signal changes shown in Fig. 2 is very similar to the one reported in the [^{14}C]iodoantipyrine study of Gerrits *et al.* (31), where the greatest CBF changes to whisker stimulation occurred at the pial layers, with layer IV showing intermediate changes and layer VI showing the smallest increases with activation (31). Although the highest BOLD changes found in the superficial layers can be explained, at least in part, by extravascular contribution from large pial veins in gradient-echo fMRI sequences (22), we are unaware of particular anatomical or vascular features that could explain the small signals observed in layer VI. Intermediate signal changes were found in the region comprised by layers IV–V, which is devoid of large vessels, but which exhibits the highest density of capillaries (38, 39). A recent study using optical imaging of intrinsic signals has related intrinsic signals to the density of capillaries in the auditory cortex of chinchillas (40). Casting studies of the cortical microvasculature in rats show a slightly lower density of capillaries in layer VI than in layer IV (41). Therefore, the small BOLD changes elicited in layer VI could be related to a lower blood volume or to a smaller metabolic and/or neuronal response.

Much controversy has existed over the last few years concerning the presence of an initial negative BOLD signal before the positive response. This early "dip" has been interpreted as an early increase in oxygen consumption before the increase in CBF (42). The time courses shown in Fig. 5*A* for a single rat suggest the presence of an early decrease in the BOLD responses from layers I–III and from layer VI before the positive response. However, this early event was not consistently observed across the nine animals studied. Its peak response was on the order of only 2 standard deviations of the mean baseline signal or less, and averaged out below statistical significance when the time courses from all animals were combined as shown in Fig. 5*B*. We and others have previously been unable to detect the early BOLD dip in this rat model of somatosensory stimulation (24, 43). In particular, the BOLD onset times reported here for layers IV–V are shorter than the ones previously obtained, arguing for an early rise in CBF. Given such early onset times, it could be possible that the BOLD dip is shifted to earlier time points and reduced in intensity, thus making it difficult to detect in this rodent model. Our present results corroborate the previous ones, and lead us to conclude that the early BOLD dip remains insignificant in the rat somatosensory cortex (44–46).

Laminar Organization of the Somatosensory Cortex and Relation to Laminar Heterogeneity of BOLD Signals. Most of the knowledge of the functional organization of layers in the rodent somatosensory cortex comes from studies of the whisker barrel field (47, 48). Such studies have established that the primary somatosensory cortex receives direct input fibers from the ventroposterior (VP) and the posterior (Po) nuclei of the thalamus. The ventroposterolateral (VPL) nucleus innervates mainly the forelimb area and the ventroposteromedial (VPM) nucleus innervates the barrel field. These thalamocortical axons terminate mainly in layer IV, but also in the deep part of layer III and sparsely in layer VI (25). Another group of thalamocortical axons connect the dorsomedial sector of the posterior nucleus (PoM) of the thalamus predominantly to layers I and Va (25). Meanwhile, layers V and VI are the main source of efferent fibers that project to several different sites of the brain (49).

Although little is know about the functional role of cortical layers, studies of receptive fields as a function of laminar depth have demonstrated an "hourglass" distribution pattern within a cortical column, which suggests that different layers are involved in different sensory information processing (50–52). A careful analysis of the spatiotemporal flow of information within the barrel cortex has demonstrated that the whisker-evoked activity in the somatosensory cortex elicits a sequence of activation that starts in layers IV and Vb (8.5 ms poststimulus), and is subsequently followed by layer III (10 ms), layers II and Va (12 ms), and by layer VI and adjacent columns (13+ ms), respectively (26, 53). Such studies have indicated both a vertical as well as a horizontal functional organization in sensory cortex, and strongly suggested that the information flows across layers within a column before being relayed to other areas of the brain. The vertical organization stems mainly from direct thalamocortical projections to layer IV, but also III and VI, through the lemniscal pathway, and to layers I and V through the paralemniscal pathway. In addition, direct projections from layer IV to the supragranular layers II and III, and from layers II and III to layer Va are know to exist (54). The horizontal organization

comes from direct intracortical spreading of the supragranular and infragranular layers (52).

The laminar specificity of BOLD onset times observed in this study is consistent with the laminar heterogeneity of onset times observed in rat whisker barrel (26, 53), albeit at a very extended time scale. These single-unit recording studies have shown a sequence of activation from the thalamus, starting in layers IV and Vb, followed by layers III, II, and Va, and finally VI and adjacent columns. It is unclear how the temporal evolution of the hemodynamic response, as probed by the BOLD signals, relates to the laminar heterogeneity of the extracellular spike recordings. The fact that BOLD onset times from layers I–III were not statistically different from the one from layer VI could be due to partial volume effects. Vascular effects could also be homogenizing onset times of functional hemodynamics. By about 1 s after onset of the stimulation, flow in the big vessels could have already increased significantly enough to flood the arterial tree, thus speeding the onset of the hemodynamic response down the functional arterioles and capillaries associated with layer VI relative to layer IV, where activity originated. Nevertheless, even though BOLD measures changes in hemodynamics, there is a growing number of examples that indicate BOLD is sensitive to events on neuronal time scales. Stimuli as short as 50 ms have been shown to give fMRI responses and careful analysis of onset times of fMRI responses have detected differences between regions at least as short as 100 ms (5). A recent report of simultaneous BOLD and local field potentials in the monkey visual cortex demonstrated that the entire BOLD response could be modeled based on a proper weighting of single-unit and multiple-unit activity (55). Ogawa *et al.* (6) recently demonstrated, in the same rat forepaw model used here, that the transient BOLD signal response to brief stimuli is additive, and proportional to a short number of repeated stimulations. In addition, they cleverly showed that the amplitude of the several seconds-long BOLD response preserves the temporal resolution of individual neuronal events separated by a few tens of milliseconds. Taken together, the above-mentioned animal-based studies, along with work presented here, provide strong evidence that the BOLD signal encodes and preserves the temporal evolution of electric neuronal events. Blood flow cannot respond as fast as electrical events. However, the vasculature could be constructed to follow electrical activity as much as possible (38, 40), making fMRI signals useful for following sequences of neural events with short latencies, such as laminar communication.

Note Added in Proof. Recently, layer-specific BOLD responses were observed in monkey visual cortex, adding to the evidence that fMRI can measure laminar signaling (56).

We acknowledge the technical assistance of Cindy Prevost, Daryl DePres, and Ruperto Villadiego. This work was supported by the National Institute of Neurological Disorders and Stroke intramural research program (Story Landis, scientific director).

1. Raichle, M. E. (1998) *Proc. Natl. Acad. Sci. USA* **95,** 765–772.
2. Buckner, R. L., Bandettini, P. A., O'Craven, K. M., Savoy, R. L., Petersen, S. E., Raichle, M. E. & Rosen, B. R. (1996) *Proc. Natl. Acad. Sci. USA* **93,** 14878–14883.
3. Friston, K. J., Fletcher, P., Josephs, O., Holmes, A., Rugg, M. D. & Turner, R. (1998) *NeuroImage* **7,** 30–40.
4. Bandettini, P. A. & Cox, R. W. (2000) *Magn. Reson. Med.* **43,** 540–548.
5. Robson, M. D., Dorosz, J. L. & Gore, J. C. (1998) *NeuroImage* **7,** 185–198.
6. Ogawa, S., Lee, T. M., Stepnoski, R., Chen, W., Zhu, X. H. & Ugurbil, K. (2000) *Proc. Natl. Acad. Sci. USA* **97,** 11026–11031.
7. Menon, R. S., Ogawa, S., Strupp, J. P. & Ugurbil, K. (1997) *J. Neurophysiol.* **77,** 2780–2787.
8. Dechent, P. & Frahm, J. (2000) *NeuroReport* **11,** 3247–3249.
9. Cheng, K., Waggoner, R. A. & Tanaka, K. (2001) *Neuron* **32,** 359–374.
10. Goodyear, B. G. & Menon, R. S. (2001) *Hum. Brain Mapp.* **14,** 210–217.
11. Kim, D. S., Duong, T. Q. & Kim, S. G. (2000) *Nat. Neurosci.* **3,** 164–169.
12. Duong, T. Q., Kim, D. S., Ugurbil, K. & Kim, S. G. (2001) *Proc. Natl. Acad. Sci. USA* **98,** 10904–10909.
13. Krause, T., Kurth, R., Ruben, J., Schwiemann, J., Villringer, K., Deuchert, M., Moosmann, M., Brandt, S., Wolf, K., Curio, G., *et al.* (2001) *Brain Res.* **899,** 36–46.
14. Bilecen, D., Scheffler, K., Schmid, N., Tschopp, K. & Seelig, J. (1998) *Hear. Res.* **126,** 19–27.
15. Giraud, A. L., Lorenzi, C., Ashburner, J., Wable, J., Johnsrude, I., Frackowiak, R. & Kleinschmidt, A. (2000) *J. Neurophysiol.* **84,** 1588–1598.
16. Talavage, T. M., Ledden, P. J., Benson, R. R., Rosen, B. R. & Melcher, J. R. (2000) *Hear. Res.* **150,** 225–244.
17. Yang, X., Hyder, F. & Shulman, R. G. (1996) *Proc. Natl. Acad. Sci. USA* **93,** 475–478.
18. Hyder, F., Behar, K. L., Martin, M. A., Blamire, A. M. & Shulman, R. G. (1994) *J. Cereb. Blood Flow Metab.* **14,** 649–655.
19. Gyngell, M. L., Bock, C., Schmitz, B., Hoehn-Berlage, M. & Hossmann, K. A. (1996) *Magn. Reson. Med.* **36,** 13–15.
20. Mandeville, J. B., Marota, J. J., Kosofsky, B. E., Keltner, J. R., Weissleder, R., Rosen, B. R. & Weisskoff, R. M. (1998) *Magn. Reson. Med.* **39,** 615–624.
21. Silva, A. C., Lee, S. P., Yang, G., Iadecola, C. & Kim, S. G. (1999) *J. Cereb. Blood Flow Metab.* **19,** 871–879.
22. Lee, S. P., Silva, A. C., Ugurbil, K. & Kim, S. G. (1999) *Magn. Reson. Med.* **42,** 919–928.
23. Mandeville, J. B., Marota, J. J., Ayata, C., Moskowitz, M. A., Weisskoff, R. M. & Rosen, B. R. (1999) *Magn. Reson. Med.* **42,** 944–951.
24. Silva, A. C., Lee, S. P., Iadecola, C. & Kim, S. G. (2000) *J. Cereb. Blood Flow Metab.* **20,** 201–206.
25. Herkenham, M. (1980) *Science* **207,** 532–535.
26. Armstrong-James, M., Fox, K. & Das-Gupta, A. (1992) *J. Neurophysiol.* **68,** 1345–1358.
27. Bandettini, P. A., Jesmanowicz, A., Wong, E. C. & Hyde, J. S. (1993) *Magn. Reson. Med.* **30,** 161–173.
28. Paxinos, G. & Watson, C. (1998) *The Rat Brain in Stereotaxic Coordinates* (Academic, San Diego).
29. Iadecola, C. (1993) *Trends Neurosci.* **16,** 206–214.
30. Gatehouse, P. D., Firmin, D. N., Collins, S. & Longmore, D. B. (1994) *Magn. Reson. Med.* **31,** 504–512.
31. Gerrits, R. J., Raczynski, C., Greene, A. S. & Stein, E. A. (2000) *Brain Res.* **864,** 205–212.
32. Malonek, D., Dirnagl, U., Lindauer, U., Yamada, K., Kanno, I. & Grinvald, A. (1997) *Proc. Natl. Acad. Sci. USA* **94,** 14826–14831.
33. Detre, J. A., Ances, B. M., Takahashi, K. & Greenberg, J. H. (1998) *Brain Res.* **796,** 91–98.
34. Matsuura, T., Fujita, H., Seki, C., Kashikura, K., Yamada, K. & Kanno, I. (1999) *Jpn. J. Physiol.* **49,** 289–296.
35. Norup, N. A. & Lauritzen, M. (2001) *J. Physiol.* **533,** 773–785.
36. Kleinfeld, D., Mitra, P. P., Helmchen, F. & Denk, W. (1998) *Proc. Natl. Acad. Sci. USA* **95,** 15741–15746.
37. Boxerman, J. L., Hamberg, L. M., Rosen, B. R. & Weisskoff, R. M. (1995) *Magn. Reson. Med.* **34,** 555–566.
38. Cox, S. B., Woolsey, T. A. & Rovainen, C. M. (1993) *J. Cereb. Blood Flow Metab.* **13,** 899–913.
39. Woolsey, T. A., Rovainen, C. M., Cox, S. B., Henegar, M. H., Liang, G. E., Liu, D., Moskalenko, Y. E., Sui, J. & Wei, L. (1996) *Cereb. Cortex* **6,** 647–660.
40. Harrison, R. V., Harel, N., Panesar, J. & Mount, R. J. (2002) *Cereb. Cortex* **12,** 225–233.
41. Mironov, V., Hritz, M. A., LaManna, J. C., Hudetz, A. G. & Harik, S. I. (1994) *Brain Res.* **660,** 73–80.
42. Malonek, D. & Grinvald, A. (1996) *Science* **272,** 551–554.
43. Marota, J. J., Ayata, C., Moskowitz, M. A., Weisskoff, R. M., Rosen, B. R. & Mandeville, J. B. (1999) *Magn. Reson. Med.* **41,** 247–252.
44. Buxton, R. B. (2001) *NeuroImage* **13,** 953–958.
45. Lindauer, U., Royl, G., Leithner, C., Kuhl, M., Gold, L., Gethmann, J., Kohl-Bareis, M., Villringer, A. & Dirnagl, U. (2001) *NeuroImage* **13,** 988–1001.
46. Vanzetta, I. & Grinvald, A. (2001) *NeuroImage* **13,** 959–967.
47. Woolsey, T. A. & Van der Loos, H. (1970) *Brain Res.* **17,** 205–242.
48. Welker, C. & Woolsey, T. A. (1974) *J. Comp. Neurol.* **158,** 437–453.
49. Wise, S. P. & Jones, E. G. (1977) *J. Comp. Neurol.* **175,** 129–157.
50. Simons, D. J. (1978) *J. Neurophysiol.* **41,** 798–820.
51. Lamour, Y., Guilbaud, G. & Willer, J. C. (1983) *Exp. Brain Res.* **49,** 46–54.
52. Chapin, J. K. (1986) *Exp. Brain Res.* **62,** 549–559.
53. Ahissar, E., Sosnik, R., Bagdasarian, K. & Haidarliu, S. (2001) *J. Neurophysiol.* **86,** 354–367.
54. Tracey, D. J. & Waite, P. M. E. (1995) in *The Rat Nervous System*, ed. Paxinos, G. (Academic, San Diego), pp. 689–704.
55. Logothetis, N. K., Pauls, J., Augath, M., Trinath, T. & Oeltermann, A. (2001) *Nature* **412,** 150–157.
56. Logothetis, N. K., Merkle, H., Augath, M., Trinath, T. & Ugurbil, K. (2002) *Neuron* **35,** 227–242.